PHYSICS

Ramped measurement technique for robust high-fidelity spin qubit readout

Daniel Keith*, Yousun Chung, Ludwik Kranz, Brandur Thorgrimsson, Samuel K. Gorman, Michelle Y. Simmons

State preparation and measurement of single-electron spin qubits typically rely on spin-to-charge conversion where a spin-dependent charge transition of the electron is detected by a coupled charge sensor. For high-fidelity, fast readout, this process requires that the qubit energy is much larger than the temperature of the system limiting the temperature range for measurements. Here, we demonstrate an initialization and measurement technique that involves voltage ramps rather than static voltages allowing us to achieve state-to-charge readout fidelities above 99% for qubit energies almost half that required by traditional methods. This previously unidentified measurement technique is highly relevant for achieving high-fidelity electron spin readout at higher temperature operation and offers a number of pragmatic benefits compared to traditional energy-selective readout such as real-time dynamic feedback and minimal alignment procedures.

INTRODUCTION

Single-electron spin qubits localized in a quantum dot have shown notable progress in recent years with the demonstration of a number of high-fidelity single- and two-qubit gates (*1*–*3*). The application of a large static magnetic field, B, lifts the degeneracy of the electron spin states, $|\downarrow\rangle$ and $|\uparrow\rangle$, by an energy given by the Zeeman interaction, $E_z = \gamma_e B$, where γ_e is the electron gyromagnetic ratio. This Zeeman energy can then be used as a method to perform single-shot initialization and measurement of the spin qubits by detuning the electrochemical potential of the quantum dot at the Fermi level of some tunnel coupled electron reservoir (*4*, *5*). Broadening of the reservoir potential due to thermal fluctuations can lead to unwanted electron tunneling, which manifests as errors, lowering the fidelity of the readout process.

To date, three main single-shot readout processes have been developed: energy-selective measurement (ESM) (*4*), time-selective measurement (TSM) (*6*), or via a second exchange-coupled ancilla quantum dot using Pauli-spin blockade (*7*, *8*). In all cases, the fidelity of the readout process is limited by the temperature of the system, which must be kept below the difference in qubit spin state energies. ESM [also known as Elzerman readout (*4*)] relies on the qubit states being separated in energy providing a state-dependent charge transition (*1*–*3*, *9*, *10*). Instead, TSM relies on the qubit states that have different tunnel rates for a particular charge transition (*6*). A nearby charge sensor is used to detect if (when) a charge transition occurs for ESM (TSM). Pauli-spin blockade readout, however, relies on measuring the singlet-triplet states in a double quantum dot, which can either be measured with a charge sensor (*7*, *11*) or dispersively (*12*–*15*). While this technique shows promise for parity measurements (*16*), it requires an additional quantum dot per qubit in contrast to ESM and TSM, where a single charge sensor is used to measure several single-spin qubits (*17*, *18*).

Standard ESM, the most common approach in quantum dot devices, relies on a three-level voltage pulse, which controls the electrochemical potential of the electron spin states ($\mu_{0\leftrightarrow\downarrow}$ and $\mu_{0\leftrightarrow\uparrow}$) around the Fermi level, E_F, of a tunnel-coupled electron reservoir (see Fig. 1A). The first voltage pulse, which we call the load phase, is used to initialize the electron spin by positioning $\mu_{0\leftrightarrow\downarrow}$ and $\mu_{0\leftrightarrow\uparrow}$ below E_F, which allows an electron to tunnel from the reservoir to the quantum dot. In the read phase, the voltage pulse quickly moves $\mu_{0\leftrightarrow\downarrow}$ and $\mu_{0\leftrightarrow\uparrow}$ such that E_F is situated between them. In this position, a spin-up electron is more likely to tunnel out to the reservoir compared to a spin-down electron. If a spin-up electron tunnels to the reservoir, then a spin-down electron can tunnel onto the quantum dot from the reservoir. This two-step tunneling process creates a "blip" in a nearby charge sensor response, which can be used to perform state-to-charge conversion of the electron spin state (see Fig. 1B) (*4*). For ESM, the density of states in the reservoir is broadened by an effective electron temperature T_e with an energy, $k_B T_e$, where k_B is the Boltzmann constant. Therefore, there is some finite probability that a detected blip is actually due to a spin-down electron tunneling to the reservoir, which causes the spin-down electron to be counted as a spin-up. These unintentional spin-down tunnel events are the main source of error when performing ESM at small magnetic fields or at high temperatures (*5*). Last, the last voltage pulse empties the electron from the quantum dot regardless of the state of the qubit by positioning $\mu_{0\leftrightarrow\downarrow}$ and $\mu_{0\leftrightarrow\uparrow}$ higher than E_F.

The ESM technique described above has allowed above 99% fidelity for electron spin readout (*17*). However, the protocol relies on the precise alignment of both $\mu_{0\leftrightarrow\downarrow}$ and $\mu_{0\leftrightarrow\uparrow}$ about E_F. The alignment procedure is usually performed by measuring a so-called "spin-tail" by varying the read level from below E_F to above E_F and then determining the optimal read level by analyzing the measurement fidelity (*5*). In a large-scale quantum computing architecture, such precise alignment accuracies may not be feasible for each and every qubit on a time scale that is allowed by charge noise (*19*). In addition, ESM requires that the ratio of the spin-up and spin-down tunnel rates to the reservoir to be ~800 corresponding to $E_Z > 13 k_B T_e$ when the reservoir is detuned midway between the Zeeman split spin states for high-fidelity readout (*5*). Recent proposals have investigated the possibility of operating spin qubits at temperatures above 1 K for increased cooling power for the cryogenic control electronics (*20*). It is therefore beneficial to have a readout protocol that can be used when $E_Z \sim k_B T_e$. To this end, we demonstrate a

Centre of Excellence for Quantum Computation and Communication Technology, School of Physics, University of New South Wales, Sydney, NSW 2052, Australia.
*Corresponding author. Email: daniel.keith@unsw.edu.au

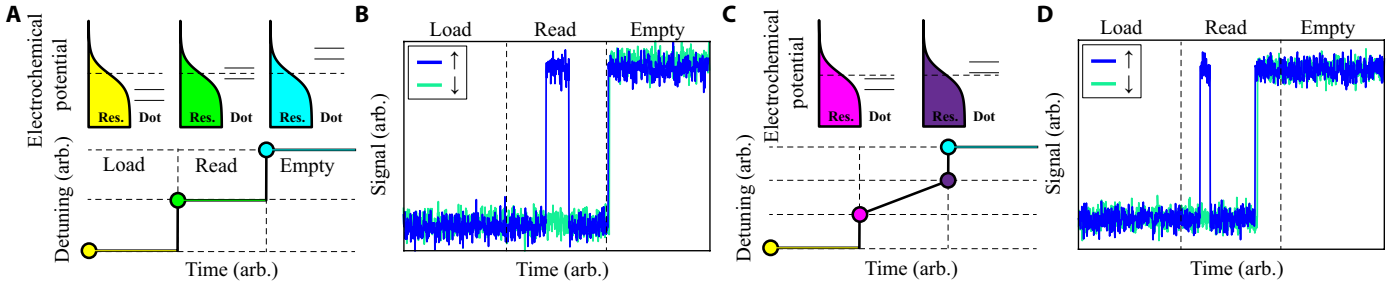

Fig. 1. Comparison of ESM and RSM techniques. (**A**) Electrochemical potential schematic for ESM and the corresponding voltage pulses used to align the electrochemical potentials of the electron spins to the Fermi level of the reservoir, E_F. The first pulse (yellow) loads an electron with a random spin state by moving both the electrochemical potentials, $\mu_{0\leftrightarrow\downarrow}$ and $\mu_{0\leftrightarrow\uparrow}$ below E_F. The spin state is then detected by a spin-dependent charge transition by moving E_F between $\mu_{0\leftrightarrow\downarrow}$ and $\mu_{0\leftrightarrow\uparrow}$ (green) such that only a spin-up electron will tunnel to the reservoir. A subsequent spin-down electron will then be loaded. Last, the electron is emptied by moving $\mu_{0\leftrightarrow\downarrow}$ and $\mu_{0\leftrightarrow\uparrow}$ above E_F (blue). (**B**) The corresponding signal from a nearby charge sensor during ESM. During the read phase, the spin-up state is detected as a characteristic blip in the charge sensor signal. (**C**) Electrochemical potential schematic for RSM. The load (yellow) and empty (blue) phases are the same as for ESM. During the read phase, the electrochemical potentials, $\mu_{0\leftrightarrow\downarrow}$ and $\mu_{0\leftrightarrow\uparrow}$, are continuously ramped from below E_F (pink) to above E_F (purple). (**D**) The corresponding charge sensor signal for RSM. A blip in the charge sensor signal before a certain threshold time indicates the presence of a spin-up electron. The charge sensor signal always reaches the maximum value before the empty phase as the spin-down electron will also tunnel out to the reservoir during the read phase.

simple initialization and measurement procedure that can be used for high-fidelity, high-temperature qubit operation.

RESULTS

Here, we demonstrate an initialization and measurement technique—which we call ramped spin measurement (RSM)—that is resilient to high-temperature/low magnetic field operation and that scales better to a large number of qubits compared to ESM. The fundamental difference between RSM and ESM, which is subtle but has a considerable impact, is that the tunnel rates of the electron spin states are continuously varied in time during the protocol rather than being fixed. Using this protocol, we show that by using RSM, we can maintain >99% spin readout fidelity for $E_Z \approx 7k_BT$, within a measurement time, $t_{meas} \approx 250t_{out/in}$, which we find to be comparable in time to ESM, but the RSM technique can be used to approximately double the temperature of ESM. In addition, the initialization procedure performed by ramping in the opposite direction to readout allows for fast initialization of the $|\downarrow\rangle$ within $t_{init} \approx 250\ t_{in}$ and with fidelities >99%. Figure 1C compares the pulse scheme for RSM to the scheme described for ESM. Importantly, during the read phase, instead of pulsing to a single detuning value and waiting for the electron spin-up state to tunnel out to the reservoir, we ramp the detuning from below E_F to above E_F. While the load and empty phases are equivalent to the ESM method, the read phase now involves determining when a blip occurred during the read phase rather than if a blip was detected (see Fig. 1D), which will alter how the RSM method should be analyzed and optimized.

The ramping fundamentally changes the way in which the spin-to-charge conversion process operates. First, the tunnel rates in and out of the quantum dot to an electron reservoir for the $|\downarrow\rangle$ and $|\uparrow\rangle$ states, $\Gamma_{\downarrow}^{in/out}$ and $\Gamma_{\uparrow}^{in/out}$, respectively, now become time dependent. Specifically, the tunnel out rates are slow at the beginning of the ramp and then increase over the duration of the ramp, while the tunnel in rates are fast at the start of the ramp and then decrease over time. Second, the time threshold is also redefined. For ESM, the time threshold is equivalent to the readout time and is chosen to determine if a blip is detected. If a blip is detected, then the qubit state is assigned to be $|\uparrow\rangle$, whereas if no blip is detected before the time threshold, then the spin state is assigned to be $|\downarrow\rangle$. However, for RSM, the time threshold is used to threshold when a blip occurred. If a blip is detected before the time threshold, then it is assigned to be $|\uparrow\rangle$, and if it occurs after, then it is assigned as $|\downarrow\rangle$ (Fig. 1D). Because the electrochemical potentials of both spin states are above E_F at the end of the ramp, there is always a step detected, that is, the electron spin has to be in either $|\uparrow\rangle$ or $|\downarrow\rangle$.

The benefit of such a ramp pulse may not be immediately obvious as there is always an optimal energy position for ESM (*5*). However, RSM is advantageous for a number of pragmatic reasons. For ESM, especially at high temperature or low magnetic field operation, the optimal detuning position is relatively far from E_F to avoid thermal fluctuations; hence, the tunnel rates to the electron reservoir are slow. The slow tunnel rates mean that the readout time becomes proportionally slow and impractical to capture the relevant tunneling events. RSM can mitigate this long readout time by attempting readout at every detuning position for a short amount of time. Therefore, the measurements can achieve high fidelity while keeping the readout time relatively short compared to the slowest possible tunnel rates. Being able to measure where the tunnel rates are slowest is particularly important because this is where the ratio between the $|\uparrow\rangle$ and $|\downarrow\rangle$ tunnel rates is greatest, and they are easily distinguished. The alignment of the RSM protocol is thus comparatively simple and fast over the traditional spin-tail measurement (*21*), because it simply performs the same pulse sequence but is insensitive to the initial and final detuning positions of the ramp as long as the entire detuning region between $\mu_{0\leftrightarrow\downarrow}$ and $\mu_{0\leftrightarrow\uparrow}$ is covered. Notably, the use of ramp pulses that have no sudden rising/falling edges that require high-frequency signals reduces the bandwidth requirements for fast pulsing thus has the consequence of being able to lower electron temperatures because additional filtering can be implemented to reduce the effect of electrical noise from external control equipment.

We model the time-varying tunnel rates of the spin states during the ramp as a nonhomogeneous Poisson process due to the independent nature of electron tunneling events. The nonhomogeneous Poisson process is defined by a rate function $\lambda^{\uparrow/\downarrow}(t)$, which describes the probability of an electron tunneling off the measured qubit at time t having not already tunneled before time t. In this case, tunneling

of an electron from the qubit to the reservoir is dictated by a Fermi distribution of temperature T_e corresponding to the effective electron temperature of the reservoir. During RSM, the detuning is ramped across the Fermi broadened electron transition during readout from an initial detuning point ϵ_0 relative to the center of the transition with a ramp rate of $r = \epsilon_{ramp}/t_{ramp}$, where ϵ_{ramp} is the change in qubit detuning relative to the reservoir, and t_{ramp} is the duration of the ramp. Hence, the rate function $\lambda^{\uparrow/\downarrow}(t)$ is given by

$$\lambda^{\uparrow/\downarrow}(t) = \frac{\Gamma}{\exp\left(-\frac{\epsilon_0^{\uparrow/\downarrow} + rt}{k_B T_e}\right) + 1} \tag{1}$$

where Γ is the maximum tunnel rate of the electron transition, k_B is the Boltzmann constant, and the electron transitions for each spin state are separated by the Zeeman energy, i.e., $\epsilon_0^{\uparrow} = \epsilon_0^{\downarrow} - E_Z$. The tunneling event distributions during RSM are equivalent to the probability density function $f^{\uparrow/\downarrow}(t)$, which, for a nonhomogeneous Poisson process can be calculated as

$$f^{\uparrow/\downarrow}(t) = \lambda^{\uparrow/\downarrow}(t) \exp\left(-\int_0^t \lambda(y)\, dy\right) \tag{2}$$

Substituting the rate equation from Eq. 1 into Eq. 2 results in the general normalized probability density function for RSM as

$$f^{\uparrow/\downarrow}(t) = \frac{\Gamma \exp(-\Gamma t)}{\exp\left(\frac{\epsilon_0^{\uparrow/\downarrow} + rt}{k_B T_e}\right) + 1} \left(\frac{\exp\left(\frac{\epsilon_0^{\uparrow/\downarrow} + rt}{k_B T_e}\right) + 1}{\exp\left(\frac{\epsilon_0^{\uparrow/\downarrow}}{k_B T_e}\right) + 1}\right)^{\frac{\Gamma k_B T_e}{r}} \tag{3}$$

Using this equation, it is possible to analytically model the electron system during RSM.

The fidelity of RSM can be quantified by the spin-up and spin-down fidelities, which are the proportion of electrons correctly identified for each spin state, respectively. Given that, for RSM, a time threshold is used to distinguish between the two spin states and hence their respective probability density functions, the spin-up (down) fidelity can be described in terms of the normalized cumulative density function (CDF) $C^{\uparrow/\downarrow}$. In general, for a given time T, the CDF is defined as

$$C^{\uparrow/\downarrow}(T) = \int_0^T f^{\uparrow/\downarrow}(t)\, dt \tag{4}$$

Hence, by substituting in Eq. 3, this results in the specific CDF $C^{\uparrow/\downarrow}(t)$ for RSM as

$$C^{\uparrow/\downarrow}(t) = 1 - \exp(-\Gamma t) \left(\frac{\exp\left(\frac{\epsilon_0^{\uparrow/\downarrow} + rt}{k_B T_e}\right) + 1}{\exp\left(\frac{\epsilon_0^{\uparrow/\downarrow}}{k_B T_e}\right) + 1}\right)^{\left(\frac{\Gamma k_B T_e}{r}\right)} \tag{5}$$

For a given value of the time threshold t, the spin-up fidelity $F^{\uparrow}(t)$ is given as $C^{\uparrow}(t)$, and the spin-down fidelity $F^{\downarrow}(t)$ is given as $1 - C^{\downarrow}(t)$. The fidelities can then be combined into a single metric, the visibility $V(t)$ as defined by

$$V(t) = F^{\uparrow}(t) + F^{\downarrow}(t) - 1 \tag{6}$$

$$= C^{\uparrow}(t) - C^{\downarrow}(t) \tag{7}$$

which will be used for optimizing the fidelity below.

To determine the measurement fidelity of the RSM using time thresholding, we determine the optimal signal value and the time value for determining when a $|\uparrow\rangle$ (or $|\downarrow\rangle$) is detected. First, with respect to the optimal time threshold t_{opt}, the maximal visibility is found when the following condition is met

$$\frac{\partial}{\partial t}(V(t_{opt})) = 0 = \frac{\partial}{\partial t}(C^{\uparrow}(t_{opt})) - \frac{\partial}{\partial t}(C^{\downarrow}(t_{opt})) \tag{8}$$

$$0 = f^{\uparrow}(t_{opt}) - f^{\downarrow}(t_{opt}) \tag{9}$$

Solving for t_{opt} we find that

$$t_{opt} = \frac{k_B T_e}{r} \log\left(\frac{X - 1}{\exp\left(\frac{\epsilon_0^{\downarrow} - E_Z}{k_B T_e}\right) - \exp\left(\frac{\epsilon_0^{\downarrow}}{k_B T_e}\right) X}\right) \tag{10}$$

where

$$X = \left(\frac{\exp\left(\frac{\epsilon_0^{\downarrow} - E_Z}{k_B T_e}\right) + 1}{\exp\left(\frac{\epsilon_0^{\downarrow}}{k_B T_e}\right) + 1}\right)^{\left(\frac{\Gamma k_B T_e - r}{r}\right)} \tag{11}$$

for compactness. Together, these equations allow the analytic determination of the optimal time threshold and measurement fidelity for a given set of RSM parameters.

In Fig. 2A, we show an example calculation of the probability and cumulative distributions for RSM used to determine the readout visibility. There are two distinct peaks offset proportional to the Zeeman energy with $B = 2$ T and $T_e = 200$ mK corresponding to the tunneling of the spin-up and spin-down spin states. The visibility is shown as the black dashed line and has a maximum at t_{opt}. Hence, calculating these distributions when matched to an experiment can be used to determine the measurement fidelity and predict how the measurement will perform in varying scenarios.

We use the model to predict how RSM behaves in comparison to ESM in the presence of charge noise. In Fig. 2B, we show 1 − visibility for the RSM, optimized ESM and ESM at zero detuning as a function of the measurement time, t relative to the electron tunnel rate, Γ. We have included the effect of integrated charge noise on all three measurement schemes. The light (dark) regions correspond to the potential fluctuation in visibility for 10 μeV (5 μeV) of charge noise. RSM is particularly robust to charge noise (with errors smaller than the line width in Fig. 2B) as the ramp pulse can be arbitrarily larger than the qubit energy splitting while retaining a similar ramp rate ensuring that the ramp always pulses sufficiently far; hence, there is practically no variation in the visibility. Therefore, despite the slower measurement time relative to Γ, RSM outperforms ESM in terms of stability to charge noise with similar visibilities. The required ramp rate (and hence readout time) scale proportionately with Γ such that the slower measurement time can be mitigated by increasing Γ by tuning device tunnel barriers. Regardless of the readout method used, the signal to noise will ultimately limit the operable measurement bandwidth.

Next, in Fig. 2 (C and D), we show the dependence of the visibility and optimal measurement time for both RSM and ESM (optimized detuning and zero detuning). As expected, for both methods, the visibility of the readout increases with increasing magnetic field electron temperature ratios (larger $\gamma_e B/k_B T_e$). RSM considerably outperforms ESM ($\epsilon = 0$) in terms of visibility but shows a similar

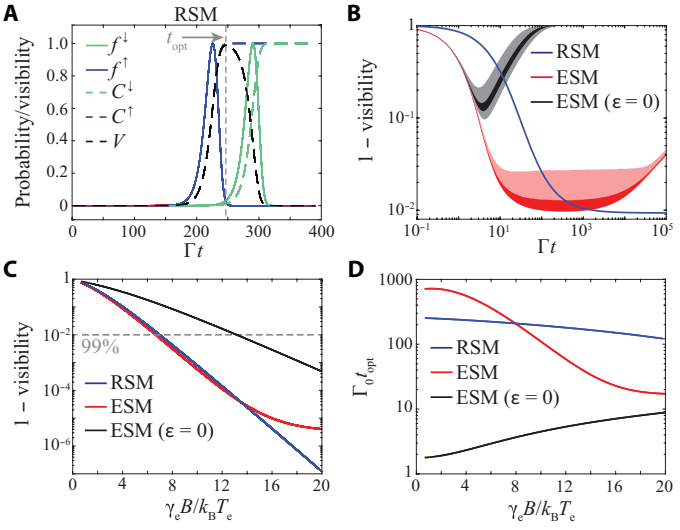

Fig. 2. Theoretical performance of ESM and RSM techniques as a function of magnetic field and temperature. (**A**) Probability densities, $f^{\uparrow/\downarrow}$, and cumulative densities, $C^{\uparrow/\downarrow}$, as a function of normalized time threshold for the spin-up (spin-down) electron in silicon for RSM at $B = 2$ T and $T_e = 200$ mK ($\gamma_e B/k_B T_e \approx 13.5$). The visibility V shows a clear peak in between the $f^{\uparrow}$ and $f^{\downarrow}$ distributions where the optimal measurement time t_{opt} is indicated by the vertical dotted line. (**B**) The complement of the visibility as a function of normalized total measurement time, Γt, for RSM (blue) and ESM for an optimized detuning, ϵ (red) and $\epsilon = 0$ (black) with $\gamma_e B/k_B T_e \approx 6.7$. The darker red and black colors correspond to the variation in visibility for an integrated 5 μeV charge noise and the lighter colored regions for 10 μeV charge noise. Because RSM is robust to noise fluctuations, there is no change in the visibility for these typical values of charge noise. (**C**) The complement of the visibility RSM (blue) and ESM for an optimized detuning, ϵ (red) and $\epsilon = 0$ (black) as a function of $\gamma_e B/k_B T_e$. Both techniques show similar visibilities over the entire range of magnetic field and temperatures investigated with RSM outperforming ESM for large magnetic field to electron temperature ratios, $\gamma_e B/k_B T_e > 15$. (**D**) The optimal measurement time for RSM (blue), optimized detuning ESM (red), and ESM with $\epsilon = 0$ (black) as a function of $\gamma_e B/k_B T_e$. The RSM technique performs better (shorter t_{opt}) than the optimized ESM for low magnetic field to electron temperature ratios; however, t_{opt} for optimized ESM drops substantially around $\gamma_e B/k_B T_e \approx 8$.

dependence to the optimized ESM; however, at high magnetic fields ($\gamma_e B/k_B T_e > 15$), RSM also outperforms the optimized ESM. While ESM ($\epsilon = 0$) performs worst in terms of visibility, it is the fastest of the methods in terms of normalized readout time Γt_{opt} all else remaining constant. For the other methods, at high $\gamma_e B/k_B T_e > 8$ values, ESM (optimized detuning) performs faster than RSM, but when $\gamma_e B/k_B T_e < 8$, the situation is reversed. More emphasis should be placed on the relative visibility performance though as the readout time is expected to scale linearly with the electron tunnel rate Γ, which can be tuned or engineered in a given device. Several take away points from Fig. 2 (C and D) are summarized in Table 1.

In Fig. 3A, we show example experimental single shot-shot traces of RSM while initializing a random electron spin state on the same electron-spin device as measured by Watson *et al.* (*17*). By monitoring the moving average of the $|\downarrow\rangle$ distribution, one can detect low-frequency detuning fluctuations in the device. The time threshold (black dashed line) can be adjusted either in real time or in post-processing by monitoring the position of the spin-down tunnel events (red crosses) to make the RSM robust to low-frequency noise during the measurement such that there will be no reduction in

Table 1. Comparison of the minimum ratio of magnetic field to electron temperature and readout times (in terms of Γ) possible with different readout methods to achieve the specified readout fidelities. While thermal limitations make it harder to reach higher fidelities, RSM and optimally tuned ESM can achieve the same fidelity as practical ESM ($\epsilon = 0$) at double the temperature (half the $\gamma_e B/k_B T_e$ value).

Method	90% Fidelity		99% Fidelity	
	$\gamma_e B/k_B T_e$	Γt_{opt}	$\gamma_e B/k_B T_e$	Γt_{opt}
ESM	3.8	651	6.7	339
ESM ($\epsilon = 0$)	7.7	4	13.2	7
RSM	4.0	266	7.0	244

readout fidelity caused by an incorrect time threshold. To determine the fidelity histograms for each trace, we determine the time at which the first step is detected, t_d, and then build a histogram of t_d for many experimental repetitions (examples are shown in Fig. 3B). The resulting histogram is shown in Fig. 3C as a function of magnetic field strength where a clear bimodal distribution can be seen. The two peaks in the histogram correspond to $|\uparrow\rangle$ and $|\downarrow\rangle$ spin states where we associate the shorter t_d events to $|\uparrow\rangle$ and the longer events to $|\downarrow\rangle$. Fits (red lines in Fig. 3C) of our previously discussed theory to these t_d histograms are used to characterize the RSM fidelity at each magnetic field strength.

In the experimental device, with optimized ramp rates, we obtain a state-to-charge conversion visibility of 99.89 ± 0.02% (99.95 ± 0.01%) at $B = 1.5$ T ($B = 0.8$ T) with an electron temperature of ~110 mK corresponding to $E_z/k_B T \approx 20.1$ ($E_z/k_B T \approx 9.8$) determined by the fit to our nonhomogeneous Poisson process (red lines in Fig. 3C). We compare this result to other single-shot electron spin readout experiments in semiconductors in Table 2. Here, RSM is performed at the lowest magnetic field, and one of the lowest values for $\gamma_e B/k_B T_e$ compared to the previous experiments, while achieving one of the highest values of the state-to-charge visibility reaching above 99%. Even at these low magnetic fields, RSM achieves some of the highest values for V, comparable to the Watson *et al.* (*17*) experiment where they deliberately tuned close to the optimal ESM point (not $\epsilon = 0$) but not as high as quoted for the experiment at 5 T (*21*) where $\gamma_e B/k_B T_e$ is more than tripled.

Last, we turn to the fidelity of the initialization of the electron spin state, which can also be improved by ramping but now in the opposite direction compared to the readout protocol. Similarly, to the readout protocol, electrons will tunnel at a different times in the ramp dependent on their spin state. For initialization, the $|\downarrow\rangle$ state will be loaded onto the quantum dot before the $|\uparrow\rangle$ state because it is lower in energy. To investigate the initialization protocol, we perform the load ramp followed by a subsequent measurement as a function of the initialization ramp time, t_{init}, see Fig. 4A. The measured proportion of $|\uparrow\rangle$ electrons as a function of t_{init} is shown in Fig. 4B. We can see that as the ramp time becomes large compared to the tunnel in times of the electron, then the qubit is deterministically loaded into $|\downarrow\rangle$. The relative population of the two spin states can be controlled continuously from ~50 to ~0% by changing the ramp time, which can be used to initialize different spin states. Specifically, in our ramped initialization experiment, ramp times less than 100 μs saturated at random initialization, while ramp

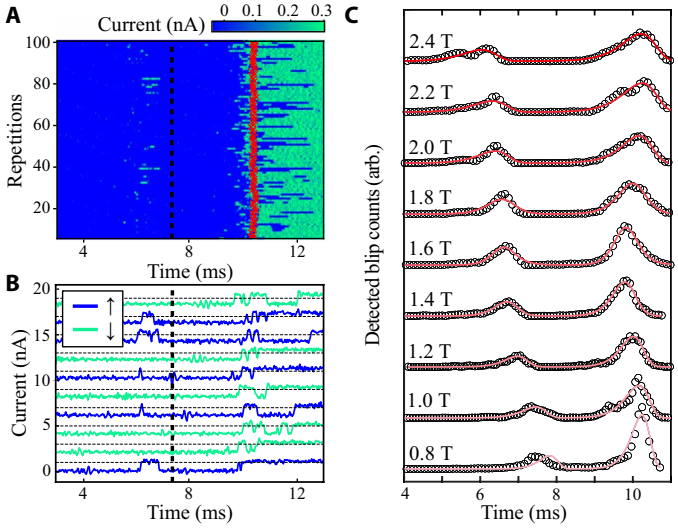

Fig. 3. Experimental demonstration of RSM. (**A**) RSM time traces showing t_{thresh} (dashed line) and a moving average of the position of the spin-down peak (red) that can be used for active feedback of the readout drift. The threshold time can also be adjusted in postprocessing to account for low-frequency voltage fluctuations of the measurement position. (**B**) Example readout traces of RSM. The detection of a blip before the dashed line time threshold, t_{thresh}, indicates that the electron was in the spin-up state (blue traces). If a tunnel event is only detected after t_{thresh}, then it is counted as a spin-down state (green traces). (**C**) The distribution (black) of initial tunnel events for 10,000 experimental repetitions of RSM while initializing a random spin-state as a function of magnetic field (offset for clarity). A clear bimodal distribution is observed where the first peak is associated with spin-up electrons and the second peak is due to spin-down electrons. The separation between the two peaks is proportional to the Zeeman energy $\gamma_e B$ of the electron spin states. Fits to the experimental distributions using a nonhomogeneous Poisson process are shown in red.

Table 2. Comparison of the ratio of magnetic field *B* to electron temperature T_e and the single-shot electron spin-to-charge visibility *V* calculated from reported experimental parameters [as reported in (*5*)] for various electron spin qubit experiments in semiconductors.

Reference	*B* [T]	T_e [mK]	$\gamma_e B/k_B T_e$	*V* [%]
(*4*) Elzerman *et al.*	10	300	9.86	79.9 ± 1.8
(*21*) Morello *et al.*	5	200	33.63	100
(*22*) Simmons *et al.*	1.85	143	17.40	97.8 ± 0.3
(*23*) Nowack *et al.*	6.5	250	7.69	77.1 ± 1.8
(*24*) Pla *et al.*	1.07	300	4.80	40.1
(*25*) Buch *et al.*	1.2	200	8.07	96.1
(*26*) Veldhorst *et al.*	1.4	150	12.55	95.7
(*9*) Watson *et al.*	1.6	160	13.45	99.4 ± 0.3
(*17*) Watson *et al.*	1.5	100	20.18	99.9
(*7*) Broome *et al.*	2.5	200	16.81	98.3 ± 1.0
(*27*) Keith *et al.*	1.5	200	10.09	97.8
This paper	1.5	110	18.34	99.89 ± 0.02
This paper	0.8	110	9.78	99.95 ± 0.01

times greater than 10 ms saturated at initializing $|\downarrow\rangle$. Intermediary time scales for the initialization ramp could be used to achieve arbitrary spin-up fractions.

We define the initialization fidelity, F^{init}, as the accuracy at which we can deterministically initialize $|\downarrow\rangle$. To accurately determine F^{init}, we need to take into account the measurement fidelity because that will contribute to the number of spin-up states we can detect. The experimentally measured spin-up count, $M^{\uparrow}$, is given by

$$M^{\uparrow} = (1 - F^{init})F^{\uparrow} + F^{init}(1 - F^{\downarrow}) \quad (12)$$

which can rearrange to obtain

$$F^{init} = \frac{F^{\uparrow} - M^{\uparrow}}{F^{\uparrow} + F^{\downarrow} - 1} \quad (13)$$

$$= \frac{F^{\uparrow} - M^{\uparrow}}{V} \quad (14)$$

Using the data from Fig. 4B and $F^{\uparrow} = 0.9979$, $F^{\downarrow} = 0.9955$, and $M^{\uparrow} = 0.0064$ at $B = 2$ T, we find $F^{init} = 0.9981$, above the 99% error threshold for fault-tolerant surface code algorithms.

We can also theoretically calculate the expected initialization fidelity F^{init} for a range of t_{ramp} values using the previously derived probability density function (Eq. 3) and the experimental fit parameters. The relevant electron tunneling rates between the reservoir and quantum dot for initialization are the complement of the relevant tunneling rates for readout. This symmetry means that both initialization and readout can be described by the same nonhomogeneous Poisson process as long as a polarity change is made to the detuning axis. Therefore, $f^{\uparrow/\downarrow}(t)$ describes the probability density function of a single spin-up (down) electron tunneling from the reservoir to the quantum dot. The biggest difference between the two processes is that initialization involves many possible electrons in the reservoir of which only one (or none) is initialized onto the quantum dot. To account for this difference when calculating the probability of initializing a spin-up (down) electron $P_{init}^{\uparrow/\downarrow}(t)$, the probability that an electron of the opposite spin had not already tunneled onto the quantum dot must be considered. Hence

$$P_{init}^{\uparrow/\downarrow}(t) = f^{\uparrow/\downarrow}(t)\left(1 - \int_0^t f^{\downarrow/\uparrow}(t')\,dt'\right) \quad (15)$$

$$= f^{\uparrow/\downarrow}(t)\,(1 - F^{\downarrow/\uparrow}(t)) \quad (16)$$

where the initialization fidelity is equal to the total probability that a spin-down electron was initialized within the ramp time, i.e.

$$F^{init} = \int_0^{t_{ramp}} P_{init}^{\uparrow}(t)\,dt \quad (17)$$

Using Eq. 17, it is possible to predict the required ramp time to initialize a certain level of initialization fidelity given a set of experiment parameters.

DISCUSSION

In summary, we have proposed and demonstrated a readout technique for semiconductor spin qubits that can achieve high readout fidelity in low-field/high-temperature contexts and is robust to electrical noise. The readout protocol is a combination of energy-selective spin readout (*4*) and time-dependent spin readout (*6*) and offers a number of pragmatic advantages over both ESM and TSM, such as

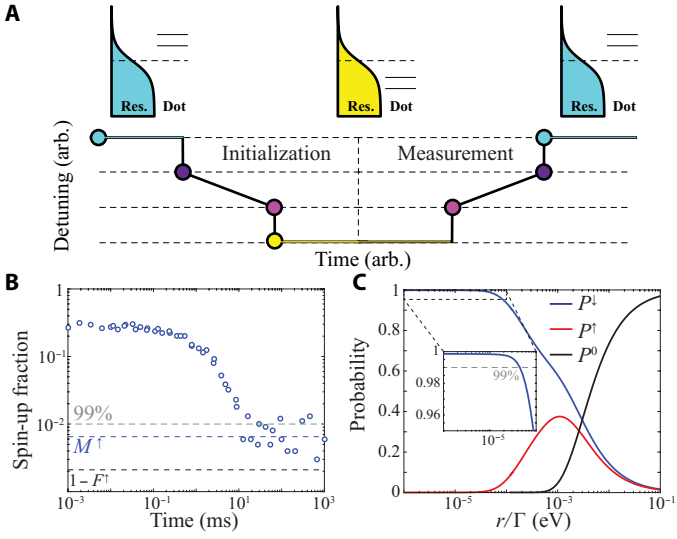

Fig. 4. Validation of the ramped spin initialization protocol. (**A**) The ramped protocol for initializing the electron spin-down state of a quantum dot. The initialization ramp is carried out in reverse order compared to the measurement procedure. The quantum dot is first unloaded, and then a detuning ramp with a rate, *r*, deterministically loads an electron spin. To validate the initialization process, we perform a subsequent RSM to measure the spin-up population. (**B**) The experimentally measured spin-up fraction as a function of ramp time for the initialization protocol. As the initialization time is increased (that is, decreased ramp rate, *r*), the spin-up population decreases until it reaches a minimum indicated by $M^{\uparrow} = 0.0064$. From previous calibration of the measurement fidelity and $M^{\uparrow}$, we can estimate the initialization fidelity using Eq. 13. (**C**) The final spin probabilities after the ramped initialization as a function of the relative ramp rate, r/Γ. For large *r*, the electron does not have enough time to tunnel from the reservoir to the quantum dot and therefore P^0 remains high. For intermediate ramp rates, both the spin-up and spin-down electrons have approximately equal occupation probabilities with $P^{\downarrow} \approx P^{\uparrow}$. Last, for slow ramp rates, the electron spin-down state is predominantly occupied since the spin-up state does not have sufficient time to tunnel onto the quantum dot. By varying *r*, a range of different mixed spin states can be initialized.

a simplified alignment scheme where we do not need to pulse to set energy level positions and can use the ground state tunnel events to instigate feedback protocols for real-time noise compensation. In addition, measurement/initialization times are kept comparable to the electron tunnel rates, and pulse bandwidth requirements are reduced due to the inherent low-frequency components making up the ramped pulses. Using this modified measurement technique, we showed that high-fidelity (>99%) spin readout can be readily performed at low magnetic field to temperature ratios (e.g., 0.8 T at 110 mK), crucial for high temperature qubit operation. Last, the reverse pulse sequence can be used to deterministically load the $|\downarrow\rangle$ ground spin state with >99% initialization fidelity or controllably load a particular mixture of $|\downarrow\rangle$ and $|\uparrow\rangle$ states. The RSM advantages over ESM will allow for simple single-shot, low magnetic field measurements that can be readily scaled to large qubit systems.

MATERIALS AND METHODS

This silicon device, as in (*17*), was fabricated using a scanning tunneling microscope (STM) to perform hydrogen lithography in ultrahigh vacuum. The surface was passivated with hydrogen, and the hydrogen was selectively removed from the surface by scanning the STM tip under lithographic conditions (3 to 5 V, 1 to 3 nA) to form a template, which was subsequently doped by exposing the surface to 20 Langmuir of PH_3 before annealing. The patterned phosphorus delta layer behaves quasi-metallically and is used to form a pair of donor dots, control electrodes, and a single electron transistor as charge detector. Last, the device was encapsulated with a ≈40-nm layer of epitaxially grown silicon with aluminum ohmic contacts used to connect to the buried phosphorus layer.

All electrical measurements of the device were performed at cryogenic temperature in a 3He/4He dilution refrigerator equipped with a 6 T superconducting magnet. The electron temperature was determined to be $T_e \approx 100$ mK from fits of RSMs to the nonhomogeneous Poisson process model. Direct current voltages/currents were applied/measured via twisted-pair wires to room temperature with voltages applied using a series of Stanford Research Systems SIM928 voltage sources, and the resulting current was measured via a Femto DLPCA-200 variable gain low-noise current amplifier. Higher-frequency waveforms were applied to a pair of control electrodes via coaxial cables and 1-kHz bias tees (100 kilohm, 1.5 nF) using a Tektronix AWG5204 arbitrary waveform generator.

REFERENCES AND NOTES

1. T. F. Watson, S. G. J. Philips, E. Kawakami, D. R. Ward, P. Scarlino, M. Veldhorst, D. E. Savage, M. G. Lagally, M. Friesen, S. N. Coppersmith, M. A. Eriksson, L. M. K. Vandersypen, A programmable two-qubit quantum processor in silicon. *Nature* **555**, 633–637 (2018).
2. D. M. Zajac, A. J. Sigillito, M. Russ, F. Borjans, J. M. Taylor, G. Burkard, J. R. Petta, Resonantly driven CNOT gate for electron spins. *Science* **359**, 439–442 (2018).
3. W. Huang, C. H. Yang, K. W. Chan, T. Tanttu, B. Hensen, R. C. C. Leon, M. A. Fogarty, J. C. C. Hwang, F. E. Hudson, K. M. Itoh, A. Morello, A. Laucht, A. S. Dzurak, Fidelity benchmarks for two-qubit gates in silicon. *Nature* **569**, 532–536 (2019).
4. J. M. Elzerman, R. Hanson, L. H. Willems van Beveren, B. Witkamp, L. M. K. Vandersypen, L. P. Kouwenhoven, Single-shot read-out of an individual electron spin in a quantum dot. *Nature* **430**, 431–435 (2004).
5. D. Keith, S. K. Gorman, L. Kranz, Y. He, J. G. Keizer, M. A. Broome, M. Y. Simmons, Benchmarking high fidelity single-shot readout of semiconductor qubits. *New J. Phys.* **21**, 063011 (2019).
6. R. Hanson, L. H. Willems van Beveren, I. T. Vink, J. M. Elzerman, W. J. M. Naber, F. H. L. Koppens, L. P. Kouwenhoven, L. M. K. Vandersypen, Single-shot readout of electron spin states in a quantum dot using spin-dependent tunnel rates. *Phys. Rev. Lett.* **94**, 196802 (2005).
7. M. A. Broome, T. F. Watson, D. Keith, S. K. Gorman, M. G. House, J. G. Keizer, S. J. Hile, W. Baker, M. Y. Simmons, High-fidelity single-shot singlet-triplet readout of precision-placed donors in silicon. *Phys. Rev. Lett.* **119**, 046802 (2017).
8. P. Harvey-Collard, B. D'Anjou, M. Rudolph, N. Tobias Jacobson, J. Dominguez, G. A. Ten Eyck, J. R. Wendt, T. Pluym, M. P. Lilly, W. A. Coish, M. Pioro-Ladrière, M. S. Carroll, High-fidelity single-shot readout for a spin qubit via an enhanced latching mechanism. *Phys. Rev. X* **8**, 021046 (2018).
9. T. F. Watson, B. Weber, M. G. House, H. Büch, M. Y. Simmons, High-fidelity rapid initialization and read-out of an electron spin via the single donor D^- charge state. *Phys. Rev. Lett.* **115**, 166806 (2015).
10. M. Veldhorst, C. H. Yang, J. C. C. Hwang, W. Huang, J. P. Dehollain, J. T. Muhonen, S. Simmons, A. Laucht, F. E. Hudson, K. M. Itoh, A. Morello, A. S. Dzurak, A two-qubit logic gate in silicon. *Nature* **526**, 410–414 (2015).
11. J. R. Petta, A. C. Johnson, J. M. Taylor, E. A. Laird, A. Yacoby, M. D. Lukin, C. M. Marcus, M. P. Hanson, A. C. Gossard, Coherent manipulation of coupled electron spins in semiconductor quantum dots. *Science* **309**, 2180–2184 (2005).
12. P. Pakkiam, A. V. Timofeev, M. G. House, M. R. Hogg, T. Kobayashi, M. Koch, S. Rogge, M. Y. Simmons, Single-shot single-gate rf spin readout in silicon. *Phys. Rev. X* **8**, 041032 (2018).
13. A. West, B. Hensen, A. Jouan, T. Tanttu, C.-H. Yang, A. Rossi, M. F. Gonzalez-Zalba, F. Hudson, A. Morello, D. J. Reilly, A. S. Dzurak, Gate-based single-shot readout of spins in silicon. *Nat. Nanotechnol.* **14**, 437–441 (2019).
14. G. Zheng, N. Samkharadze, M. L. Noordam, N. Kalhor, D. Brousse, A. Sammak, G. Scappucci, L. M. K. Vandersypen, Rapid gate-based spin read-out in silicon using an on-chip resonator. *Nat. Nanotechnol.* **14**, 742–746 (2019).

15. M. Urdampilleta, D. J. Niegemann, E. Chanrion, B. Jadot, C. Spence, P.-A. Mortemousque, C. Bäuerle, L. Hutin, B. Bertrand, S. Barraud, R. Maurand, M. Sanquer, X. Jehl, S. De Franceschi, M. Vinet, T. Meunier, Gate-based high fidelity spin readout in a CMOS device. *Nat. Nanotechnol.* **14**, 737–741 (2019).
16. A. E. Seedhouse, T. Tanttu, R. C. C. Leon, R. Zhao, K. Y. Tan, B. Hensen, F. E. Hudson, K. M. Itoh, J. Yoneda, C. H. Yang, A. Morello, A. Laucht, S. N. Coppersmith, A. Saraiva, A. S. Dzurak, Pauli blockade in silicon quantum dots with spin-orbit control. *PRX Quantum* **2**, 010303 (2021).
17. T. F. Watson, B. Weber, Y.-L. Hsueh, L. C. L. Hollenberg, R. Rahman, M. Y. Simmons, Atomically engineered electron spin lifetimes of 30 s in silicon. *Sci. Adv.* **3**, e1602811 (2017).
18. C. D. Hill, E. Peretz, S. J. Hile, M. G. House, M. Fuechsle, S. Rogge, M. Y. Simmons, L. C. L. Hollenberg, A surface code quantum computer in silicon. *Sci. Adv.* **1**, e1500707 (2015).
19. L. Kranz, S. K. Gorman, B. Thorgrimsson, Y. He, D. Keith, J. G. Keizer, M. Y. Simmons, Exploiting a single-crystal environment to minimize the charge noise on qubits in silicon. *Adv. Mater.* **32**, 2003361 (2020).
20. L. M. K. Vandersypen, H. Bluhm, J. S. Clarke, A. S. Dzurak, R. Ishihara, A. Morello, D. J. Reilly, L. R. Schreiber, M. Veldhorst, Interfacing spin qubits in quantum dots and donors—Hot, dense, and coherent. *npj Quantum Inf.* **3**, 34 (2017).
21. A. Morello, J. J. Pla, F. A. Zwanenburg, K. W. Chan, K. Y. Tan, H. Huebl, M. Mottonen, C. D. Nugroho, C. Yang, J. A. van Donkelaar, A. D. C. Alves, D. N. Jamieson, C. C. Escott, L. C. L. Hollenberg, R. G. Clark, A. S. Dzurak, Single-shot readout of an electron spin in silicon. *Nature* **467**, 687–691 (2010).
22. C. B. Simmons, J. R. Prance, B. J. Van Bael, T. S. Koh, Z. Shi, D. E. Savage, M. G. Lagally, R. Joynt, M. Friesen, S. N. Coppersmith, M. A. Eriksson, Tunable spin loading and T_1 of a silicon spin qubit measured by single-shot readout. *Phys. Rev. Lett.* **106**, 156804 (2011).
23. K. C. Nowack, M. Shafiei, M. Laforest, G. E. D. K. Prawiroatmodjo, L. R. Schreiber, C. Recihl, W. Wegscheider, L. M. K. Vandersypen, Single-shot correlations and two-qubit gate of solid-state spins. *Science* **333**, 1269–1272 (2011).
24. J. J. Pla, K. Y. Tan, J. P. Dehollain, W. H. Lim, J. J. L. Morton, D. N. Jamieson, A. S. Dzurak, A. Morello, A single-atom electron spin qubit in silicon. *Nature* **489**, 541–545 (2012).
25. H. Buch, S. Mahapatra, R. Rahman, A. Morello, M. Y. Simmons, Spin readout and addressability of phosphorus-donor clusters in silicon. *Nat. Commun.* **4**, 2017 (2013).
26. M. Veldhorst, J. C. C. Hwang, C. H. Yang, A. W. Leenstra, B. de Ronde, J. P. Dehollain, J. T. Muhonen, F. E. Hudson, K. M. Itoh, A. Morello, A. S. Dzurak, An addressable quantum dot qubit with fault-tolerant control-fidelity. *Nat. Nanotechnol.* **9**, 981–985 (2014).
27. D. Keith, M. G. House, M. B. Donnelly, T. F. Watson, B. Weber, M. Y. Simmons, Single-shot spin readout in semiconductors near the shot-noise sensitivity limit. *Phys. Rev. X* **9**, 041003 (2019).

Acknowledgments

Funding: The research was supported by the Australian Research Council Centre of Excellence for Quantum Computation and Communication Technology (project number CE170100012) and Silicon Quantum Computing Pty Ltd. M.Y.S. acknowledges an Australian Research Council Laureate Fellowship. This work was performed in part at the NSW node of the Australian National Fabrication Facility. **Author contributions:** D.K., Y.C., and L.K. measured the experimental data. D.K. derived the analytical expressions with helpful discussion from S.K.G. and B.T. The manuscript was written by D.K., S.K.G., and M.Y.S with input from all other authors. M.Y.S. supervised the project. **Competing interests:** M.Y.S. is a director of the company Silicon Quantum Computing Pty Ltd. D.K., S.K.G., Y.C., L.K., B.T., and M.Y.S. are inventors on a pending patent related to this work filed by Silicon Quantum Computing Pty Ltd. (no. AU2021904192, filed 22 December 2021). The authors declare that they have no other competing interests. **Data and materials availability:** All data needed to evaluate the conclusions in the paper are present in the paper and/or the Supplementary Materials.

Submitted 17 March 2022
Accepted 21 July 2022
Published 7 September 2022
10.1126/sciadv.abq0455